Process noise quantification in Kalman filters with application to electrochemical Lithium-ion battery state estimation

Ross M. Weber, Robert Spragg, Kenneth Hoffmann, Dr. Simona Onori *, *Senior Member, IEEE*

***Abstract*— Accurate state estimation of Lithium-ion batteries (LIBs) can enable improved hybrid and electric vehicles. A Battery Management System (BMS) can use electrochemical models in conjunction with Kalman filter approaches to estimate internal battery states from current and voltage measurements. For Kalman filters, the process noise is assumed to be Gaussian and independent across states, resulting in a diagonal covariance matrix. To the best of our knowledge, these assumptions have never been validated for battery dynamics, nor has any detailed calculation of variance of each model state been presented. This paper proposes a novel method for quantifying process noise in electrochemical battery models that can be generalized to other system applications. The method is derived analytically by mapping a "true" high-fidelity model to a reduced model and comparing differences in concentration states. The electrochemical model used is an enhanced Single Particle Model (eSPM), where parameters were experimentally identified for a Li-NMC cell. An investigation of process noise carried out using the proposed approach shows that the covariance matrix is not diagonal and gaussian only in first approximation (but only for the diagonal terms).**

I. Introduction

Lithium-ion batteries (LIBs) have become ubiquitous in portable electronics due to their high energy density, but they remain a bottleneck in the development of hybrid and electric vehicles [1]. An onboard Battery Management System (BMS) takes current and voltage measurements and run algorithms to estimate internal states such as state-of-charge (SOC) and state-of-health (SOH) to ensure safe operation and prolonged life [2].

Electrochemical LIB models are preferred to empirical models as they embed physical information that cannot be directly measured. The most commonly used electrochemical model is the Doyle-Fuller-Newman (DFN) model, which considers the pore-scale diffusion, reaction, and electromigration of lithium particles [3]. It is derived via upscaling Poisson-Nernst-Planck equations to capture particle dynamics, and Butler-Volmer reaction kinetics are applied at the solid-electrolyte interface (SEI) to determine the intercalation flux. The drawback of the model is that it is governed by sets of nonlinear coupled partial differential equations (PDEs), which prohibits their real-time application.

A common simplification of electrochemical models is the Single Particle Model (SPM) [4], which treats each electrode as a single spherical particle and considers only the radial diffusion within these particles. The electrolyte is considered constant in space and time, an assumption that is violated at high C-rates of operation. To overcome this, the enhanced Single Particle Model (eSPM) was developed [4], which incorporates electrolyte dynamics for improved accuracy.

Plett introduced an extended Kalman filter (EKF) for LIB state estimation using an equivalent circuit model [5]. EKFs have also been applied to electrochemical models for SOC estimation [6]. In all such applications, assumptions are made, without verification, that process noise for each state is *(1) Gaussian* and *(2) independent and identically distributed*.

Unfortunately, those assumptions are assumed *as is* without any verification about their validity for the application under study. Practically speaking, this results in having a diagonal covariance matrix. This assumption, however, is in general counterintuitive, as it implies that the states of a dynamical system are mutually uncorrelated, which is not always the case.

For example, in the eSPM, states are lithium concentrations in specific regions of the electrode, and error can be introduced by incorrectly estimating either diffusive transport or intercalation flux. In the former case, over-calculating diffusion from state A to state B would lead to an underestimate of state A concentration and an overestimate of state B concentration, resulting in a negative correlation and covariance value. On the other hand, incorrectly estimating the intercalation flux into or out of the particle would introduce error in the same direction for all states, resulting in a positive covariance value. In either case, the error across states is not independent, so the assumption of diagonal covariance is not verified.

Correctly characterizing process noise is crucial for accurate state estimation, as underestimating it will cause overconfidence in the model and the state predictions could diverge from the real values, but overestimating it will lead to overfitting towards measurement noise. This paper explores the validity of these assumptions made about process noise for battery electrochemical dynamics by presenting an analytically derived mapping method .

This paper is organized as follows. Section II describes the battery electrochemical model, the state-space formulation, and parameter identification. Section III discusses the observer design, including the novel mapping method for characterizing noise and the EKF algorithm. Section IV investigates the process noise on drive-cycle data using the novel approach.

Ross M. Weber and S. Onori are with the Department of Energy Resources Engineering, Stanford University, Robert Spragg is with the Department of Civil Engineering, Stanford University, Kenneth Hoffman is with the Department of Mechanical Engineering, Stanford University

*corresponding author, sonori@stanford.edu.

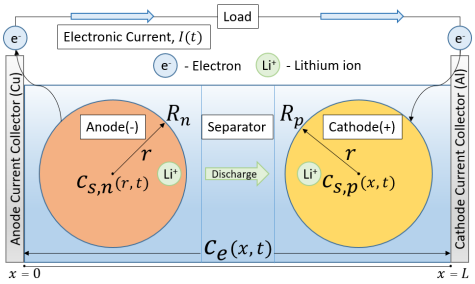

Fig. 1: Diagram detailing the eSPM. During discharge, lithium-ions diffuse out of the anode and through the separator to the cathode.

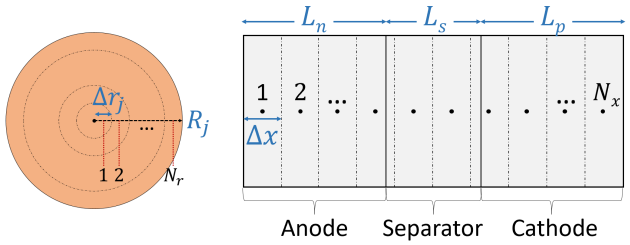

Fig. 2: Discretization of (a) electrode into N_r spherical shells of thickness Δr_j and (b) electrolyte into N_x rectangular prisms of width Δx.

II. Lithium-ion Battery Model

A. Enhanced Single Particle Model (eSPM)

The eSPM [4] is an electrochemical LIB model derived by simplifying the DFN model [3]. As shown in Figure 1, it approximates each electrode as a single spherical particle and considers lithium diffusion across the electrolyte. Solid phase lithium concentration, $c_{s,j}$, is governed by Fick's Law,

$$\frac{\partial c_{s,j}}{\partial t}(r,t) = \frac{1}{r^2}\frac{\partial}{\partial r}\left[D_{s,j}r^2\frac{\partial c_{s,j}}{\partial r}(r,t)\right], \quad (1)$$

with boundary conditions

$$\frac{\partial c_{s,j}}{\partial r}(0,t) = 0, \frac{\partial c_{s,j}}{\partial r}(R_j,t) = \frac{1}{D_{s,j}FA_{cell}a_jL_j}I(t), \quad (2)$$

where $j = (n,p)$ denotes anode or cathode. Electrolyte concentration, c_e, is resolved by:

$$\frac{\partial c_e(x,t)}{\partial t} = \frac{\partial}{\partial x}\left[\frac{D_{e,j}^{eff}}{\epsilon_{e,j}}\frac{\partial c_e(x,t)}{\partial x}\right] + z_j\frac{(1-t_0^+)}{\epsilon_{e,j}FA_{cell}L_j}I(t), \quad (3)$$

with boundary conditions

$$\frac{\partial c_e}{\partial x}(0,t) = 0, \frac{\partial c_e}{\partial x}(L,t) = 0, \quad (4)$$

where F is Faraday's constant and $z_j = -1$ in the anode, 0 in the separator, and 1 in the cathode to describe relationship between input current, defined as positive during discharge, and intercalation flux direction. The effective diffusion coefficient, $D_{e,j}^{eff}$, is found using the Bruggeman relationship [7], $D_{e,j}^{eff} = D_e\epsilon_{e,j}^{1.5}$.

The PDEs describing the eSPM are reduced to a set of Ordinary Differential Equations (ODEs) by using the Finite Difference Method (FDM). The electrode particles are discretized radially into N_r hollow spherical shells. The electrolyte, which spans the entire cell, is discretized into N_x nodes, which are equally-spaced rectangular prisms between the current collectors. The model thus has $2N_r+N_x$ states, where each state represents a lithium concentration (mol/m^3) in a fixed volume. The FDM discretization is shown in Figure 2. This discretization method of the electrolyte results in two states that include the intersection of an electrode and the separator. For these states, domain-dependent parameters, such as $\epsilon_{e,j}$, are linearly interpolated based on the relative volumes in each domain.

The predicted output voltage, $V(t)$ of the eSPM depends on the open circuit voltage, V_{oc}, the electrode overpotentials, η_j, the electrolyte voltage drop, V_e, and the voltage across the contact resistance, R_cI, as follows,

$$V(t) = V_{oc,p}(\theta_p) - V_{oc,n}(\theta_n) + \eta_p(t) - \eta_n(t) + V_e(t) - R_cI(t). \quad (5)$$

The V_{oc} of the anode and cathode are derived empirically and are given by [4]

$$\begin{aligned} V_{oc,n}(\theta_n) = {} & 0.15 + 0.85e^{-61.8\,\theta_n} + 0.38e^{-666\,\theta_n} \\ & - e^{(39.4\,\theta_n - 41.9)} - 0.031\tan^{-1}(25.6\,\theta_n - 4.1) \\ & - 0.0094\tan^{-1}(32.5\,\theta_n - 15.7), \end{aligned} \quad (6a)$$

$$V_{oc,p}(\theta_p) = -11\,\theta_p^4 + 24\,\theta_p^3 - 17\,\theta_p^2 + 2.6\,\theta_p + 4.6, \quad (6b)$$

where $\theta_j = c_{ss,j}/c_{s,max,j}$ is the surface stoichiometric coefficient. The electrode overpotentials, η_j, are given by

$$\eta_j(t) = \frac{2R_gT}{F}\sinh^{-1}\left(\frac{I(t)}{2a_jA_{cell}L_ji_{0,j}(t)}\right), \quad (7)$$

where R_g is the ideal gas constant, T is cell temperature, and a_j is the specific interfacial surface area. The exchange current density, $i_{0,j}$ is equal to:

$$i_{0,j}(t) = k_j\sqrt{c_{ss,j}(t)c_{e,0}(t)[c_{s,max,j} - c_{ss,j}(t)]} \quad (8)$$

where $c_{ss,j}$ is the surface concentration in the outermost electrode shell. The electrolyte voltage (V_e) is equal to

$$V_e(t) = -\frac{L_n+2L_s+L_p}{2A_{cell}K_e^{eff}}I(t) + \frac{2R_gT}{F}(1-t_0^+)\ln\frac{c_e^+(t)}{c_e^-(t)}, \quad (9)$$

where $c_e^{\pm}(t)$ is the electrolyte concentration at the positive and negative current collectors. The effective conductivity, K_e^{eff}, is determined from the Bruggeman relation, $K_e^{eff} = K_e\bar{\epsilon}_e^{1.5}$, where $\bar{\epsilon}_e$ is the average porosity in the cell.

B. State-space Formulation

The eSPM model is discretized using the FDM and put into state-space representation:

$$\begin{bmatrix}\dot{x}_n\\ \dot{x}_p\\ \dot{x}_e\end{bmatrix} = \begin{bmatrix}A_{s,n} & 0 & 0\\ 0 & A_{s,p} & 0\\ 0 & 0 & A_e\end{bmatrix}\begin{bmatrix}x_n\\ x_p\\ x_e\end{bmatrix} + \begin{bmatrix}B_{s,n}\\ B_{s,p}\\ B_e\end{bmatrix}u, \quad (10a)$$

$$y = h(x_n, x_p, x_e, u), \quad (10b)$$

where the input, u, is current, $I(t)$. The output, y, is voltage, $V(t)$, and $h(x_n, x_p, x_e, u)$ is the RHS Equation 5, and the state vectors, x_n, x_p, and x_e represent the lithium concen-

Parameter	Anode	Separator	Cathode
Thickness, L [μ m]	52.97	20.78	37.74
Particle radius, R [μm]	8.624		8.872
Electrode plate area, A_{cell} [m^2]		0.1005	
Active material volume fraction, ϵ_s	0.6078		0.5615
Porosity (electrolyte phase volume fraction), ϵ_e	0.3235	0.4945	0.3518
Maximum solid phase concentration, $c_{s,max}$ [mol/m^3]	35,154		59,650
Stoichiometry at 0% SOC, $\theta_{0\%}$	0.0711		0.9256
Stoichiometry at 100% SOC, $\theta_{100\%}$	0.7125		0.3486
Average electrolyte concentration, $\bar{c_e}$ [mol/m^3]		1,025	
Kinetic reaction rate, k [A m$^{2.5}$ / mol$^{1.5}$]	1.298e^{-6}		4.610e^{-6}
Li$^+$ transference number, t_0^+		0.3512	
Solid phase Li diffusion coefficient, D_s [m^2/s]	1.426e^{-13}		1.236e^{-13}
Electrolyte phase Li$^+$ diffusion coefficient, D_e [m^2/s]		1.632e^{-10}	
Electrolyte conductivity, K_e [S/m]		3.841	
Contact resistance, R_c [Ω]		3.039e^{-5}	

TABLE I: Experimentally identified parameters for the eSPM model on a Li-NMC cell using MATLAB Genetic Algorithm.

trations in the anode, cathode, and electrolyte respectively:

$$x_n = \begin{bmatrix} c_{s,n,1} \\ c_{s,n,2} \\ \vdots \\ c_{s,n,N_r} \end{bmatrix}, x_p = \begin{bmatrix} c_{s,p,1} \\ c_{s,p,2} \\ \vdots \\ c_{s,p,N_r} \end{bmatrix}, x_e = \begin{bmatrix} c_{e,1} \\ c_{e,2} \\ \vdots \\ c_{e,N_x} \end{bmatrix}. \quad (11)$$

The state and input matrices are computed as

$$A_{s,j} = \begin{bmatrix} -2 & 2 & 0 & 0 & \dots & 0 \\ \frac{1}{2} & -2 & \frac{3}{2} & 0 & \dots & 0 \\ 0 & \frac{2}{3} & -2 & \frac{4}{3} & \dots & 0 \\ \vdots & \vdots & \ddots & \ddots & \ddots & \vdots \\ 0 & 0 & 0 & \dots & 2 & -2 \end{bmatrix} \frac{D_{s,j}}{(\Delta r_j)^2}, \quad (12a)$$

$$A_e = \begin{bmatrix} -1 & 1 & 0 & \dots & 0 \\ 1 & -2 & 1 & \dots & 0 \\ \vdots & \ddots & \ddots & \ddots & \vdots \\ 0 & \dots & 1 & -2 & 1 \\ 0 & \dots & 0 & 1 & -1 \end{bmatrix} \frac{D_{e,j}^{eff}}{(\Delta x)^2}, \quad (12b)$$

$$B_{s,j} = \begin{bmatrix} 0 \\ \vdots \\ 0 \\ 2 + \frac{2}{N_r} \end{bmatrix} \frac{z_j}{\Delta r_j F A_{cell} a_{s,j} L_j}, \quad (12c)$$

$$B_e = \begin{bmatrix} 1 \\ \vdots \\ 1 \end{bmatrix} z_j \frac{(1 - t_0^+)}{\epsilon_{e,j} F A_{cell} L_j}. \quad (12d)$$

Domain-depended coefficients such as $\epsilon_{e,j}$ will vary by row in A_e and B_e, which correspond to a specific rectangular prisms of the electrolyte as depicted in Figure 2b.

C. Parameter Identification

The eSPM model was parameterized experimentally using a constant 1C-rate discharge input profile. The data was taken using a 2Ah 3.6V Li-NMC cell. A genetic algorithm in MATLAB was used to identify 25 eSPM parameters, which are given in Table I. Experimental data was also taken for two drive-cycle datasets, US06 and UDDS. The root-mean-squared error (RMSE) with respect to measured voltage for these parameters was found to be 9.7mV (0.26%) and 13.9mV (0.35%) for the US06 and UDDS respectively.

III. Observer Design

A. Observability

The observer uses voltage measurements taken at discrete time intervals to update the state estimate. Electrochemical-based estimators for LIBs suffer from weak observability when estimating lithium concentrations in both electrodes and the electrolyte concurrently [8]. This is because the output voltage is measured as the difference between two electrode potentials, which are each nonlinear functions of concentration (Equation 6), so the voltage in a single electrode is not discernible. To circumvent this issue, the number of lithium moles is assumed to be conserved, which establishes algebraic relationships between concentration fluxes entering and leaving each domain [6]. These assumed relationships are invalid under battery aging, as lithium ions get consumed by side reactions resulting in SEI layer growth or lithium plating [9].

In this work, the observer resolves only the cathode concentration states. Therefore, the state-space model, which is now in discrete-time formulation, reduces to

$$x_{p,k} = A_k x_{p,k-1} + B_k u_k + w_k, \quad (13a)$$

$$y_k = h_k(x_{p,k}, u_k) + v_k. \quad (13b)$$

where k is the time step, and w_k and v_k are the process and measurement noise respectively, which will be discussed in Section III-B. A_k and B_k are determined by:

$$A_k = \Delta t_k A_{s,p} + I, \quad (14a)$$

$$B_k = \Delta t_k B_{s,p}, \quad (14b)$$

where I is the identity matrix and Δt_k is the length of time interval. The anode concentration is computed by the

following relationship [6]:

$$\frac{\theta_{n,k} - \theta_{n,0\%}}{\theta_{n,100\%} - \theta_{n,0\%}} = \frac{\theta_{p,k} - \theta_{p,0\%}}{\theta_{p,100\%} - \theta_{p,0\%}}. \tag{15}$$

For the electrolyte, Equation 9 shows that only current collector concentrations are needed, which are at the first and last discretization nodes. This is done by assuming that the deviation from the average electrolyte concentration in these regions is equal to the lithium that entered or left the electrode in this node at each time step:

$$c_{e,k}^{\pm} = \bar{c_e} \mp \frac{u_k}{F A_{cell} a_j L_j} \frac{\Delta t_k}{\Delta x}. \tag{16}$$

The stability of this term is ensured as Von Neumann stability analysis requires that Δt decreases with Δx^2 for the FDM.

The voltage function, $h_k(x_p, u)$ in Equation 13 now only depends on x_p because x_n and x_e are defined as functions of x_p through Equations 15 and 16. Although electrolyte diffusion is not explicitly resolved, electrolyte dynamics are considered during Equation 9, so this formulation is still an observable eSPM. Finally, the SOC is determined from the cathode concentration:

$$SOC = \frac{\frac{c_{s,bulk,p}}{c_{s,max,p}} - \theta_{0\%,p}}{\theta_{100\%,p} - \theta_{0\%,p}}. \tag{17}$$

B. Noise Quantification

Kalman filter implementation requires that both process and measurement noises are Gaussian. In Equation 13 the process noise, w_k, is defined as the uncertainty that is introduced by the model, and the measurement noise, v_k, is the uncertainty from the sensor readings at time step k. While measurement noise is straightforward and well-defined when sensor readings are available, process noise is difficult to quantify, yet the large body of literature in the field simply assumes Gaussian and uncorrelated process noise states without provided justification.

In this paper, we present a method to characterize the nature of the process error. The process noise indicates how trustworthy the equations used to represent the system are with respect to the real dynamics. This is usually very hard to asses, and it is often the case to treat the process noise covariance matrix as a tuning parameter to adjust the gain of the Kalman filter.

We consider the process noise as the difference between the high fidelity state vector and the dynamics predicted by the reduced model at each time step. For example, a *reduced* eSPM with fewer discretizations truncates dynamics and introduces error. In doing so, both the unmodeled dynamics and stochastic noise are being lumped together, with input dependence on the estimation algorithm being a major drawback.

In the proposed method, process noise for a *reduced* model with N states is quantified by first running a "true", *high-fidelity* model with $M = PN$ states, with $P > 1$ defined as an integer, resulting in a vector $x_k^{hf} \in \mathbb{R}^M$ for each time step. The linear transformation $\mathbf{g} : \mathbb{R}^M \to \mathbb{R}^N$ is then defined by:

$$x_k^{red} = \mathbf{g}(x_k^{hf}) = G x_k^{hf}, \tag{18}$$

where $G \in \mathbb{R}^{N \times M}$ is given by:

$$G = \begin{bmatrix} \frac{\langle V_1^{hf} \rangle}{\langle V_1^{red} \rangle} & \dots & \frac{\langle V_P^{hf} \rangle}{\langle V_1^{red} \rangle} & 0 & & \dots & 0 \\ \vdots & & & \ddots & & & \vdots \\ 0 & \dots & & 0 & \frac{\langle V_{M-P+1}^{hf} \rangle}{\langle V_N^{red} \rangle} & \dots & \frac{\langle V_M^{hf} \rangle}{\langle V_N^{red} \rangle} \end{bmatrix}, \tag{19}$$

where $\langle V_i^{hf} \rangle$ and $\langle V_i^{red} \rangle$ represent the volumes of the i^{th} spherical shell in the high fidelity and reduced model, respectively. Thus, building the matrix G can be thought of as a 3 step process: First, each state (mol/m^3) in the high-fidelity model is multiplied by its respective volume. Second, each set of P elements are summed together, resulting in N values with units of mol. Third, each element is divided by the volume of the shells in the reduced model (or equivalently, the sum of P high-fidelity shell volumes) to obtain N concentration states to be compared against the reduced model. This process is necessary in LIB applications because concentrations in mol/m^3 cannot be summed without accounting for volume. If the volume of the shells were uniform, the nonzero entries of G would be $1/P$.

The motivation for this is that each set of P states in the high-fidelity model represents the same volume element as a single state in the reduced model and thus can be combined together using the transformation, $\mathbf{g}$, into one state. This step, which we call "mapping", results in new vector, $x_k^{red} \in \mathbb{R}^N$ that represents the "true" state for the reduced model at each time step. Then, process noise at each time step is the truncation error that would be introduced by the reduced model and Q is the covariance of the noise over time:

$$w_k = \mathbf{g}(x_k^{hf}) - [A_k x_{k-1}^{red} + B_k u_k], \tag{20a}$$

$$Q = cov(w), \tag{20b}$$

where $A_k \in \mathbb{R}^{N \times N}$ & $B_k \in \mathbb{R}^N$ represent the reduced model. A flowchart detailing this process in shown in Figure 3.

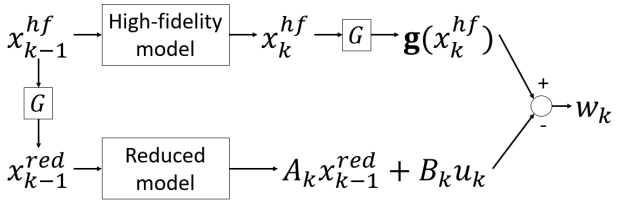

Fig. 3: Flowchart describing process noise quantification at time step k.

C. Extended Kalman Filter

An *a priori* estimate of the state, $x_{p,k}^-$, voltage, V_k^-, and covariance, P_k^-, are computed as follows,

$$x_{p,k}^- = A_k x_{p,k-1} + B_k u_k, \quad V_k^- = h(x_{p,k}^-, u_k), \tag{21a}$$

$$P_k^- = A_k P_{k-1} A_k^T + Q. \tag{21b}$$

The innovation, e_k, is computed by taking the difference of the measured voltage, V_k^{exp}, and the *a priori* estimate:

$$e_k = V_k^{exp} - V_k^-. \tag{22}$$

The linearized output matrix and Kalman gain, K_k, are given by:

$$H_k = \frac{\partial h}{\partial x}(x_{p,k}^-, u_k), \tag{23a}$$

$$K_k = P_k^- H_k^T (H_k P_k^- H_k^T + R)^{-1}, \tag{23b}$$

where R is the variance of the measurement noise. The state vector, voltage, and covariance matrix estimates are then updated using the Kalman gain and innovation:

$$x_{p,k} = x_{p,k}^- + K_k e_k, \quad V_k = h(x_{p,k}, u_k), \tag{24a}$$

$$P_k = (I - K_k H_k) P_k^-. \tag{24b}$$

IV. Results and Discussion

A. Process Noise Characterization

The method presented for quantifying process error was applied using an eSPM (Equation 10) with $M = 30$ cathode states as the high-fidelity model and an observable eSPM (Equation 13) with $N = 3$ cathode shells as the reduced model ($P = 10$). The cathode states from the high-fidelity model were then compared with the reduced model using Equation 20 to quantify the process noise. The input profile used for calibrating the noise is the US06 drive cycle. A correlation plot for all states is shown in Figure 4. State 1 is defined as the innermost shell of the reduced model and State 3 is the outermost.

The first common assumption when quantifying process noise for electrochemical LIB models is that the noise is zero-mean Gaussian, meaning that the model has no tendency to either over predict or under predict concentration states. To examine the validity of this assumption, histograms of the process noise for each state are shown along the diagonal plots of Figure 4. For each histogram, a z-test demonstrated that the noise was 27.4%, 80.0%, and 97.0% Gaussian for States 1-3, respectively. Clear, the inner shell error is not very Gaussian, but the outer states with the significantly higher variance can be considered roughly Gaussian, especially for the state with the highest variance.

The next common assumption is that process noise for each state is mutually uncorrelated. Figure 4 demonstrates that this assumption is invalid, as all states showed a positive correlation with each other. This means that when the model overestimates lithium concentration in one shell, it is likely to overestimate lithium concentration in all other shells. The full covariance matrix was found to be:

$$Q = 1e\text{–}2 \begin{bmatrix} 0.32 & 0.10 & 0.08 \\ 0.10 & 1.42 & 0.62 \\ 0.08 & 0.62 & 40.8 \end{bmatrix}. \tag{25}$$

This covariance matrix and the correlation coefficients, R in Figure 4, demonstrate that the off-diagonal elements, especially those for adjacent and outer shells, need to be considered. This pattern, which is found for all N and P, can be explained by intercalation flux uncertainties being the dominant source of model error. When the flux is incorrectly computed, error is introduced in the outermost state and propagates inward, resulting in positive correlations for all states.

B. Implementation in EKF

The EKF with process noise covariance matrix quantified as presented in this paper, Q_f, is applied to a UDDS drive cycle, and compared with an EKF where process noise is diagonal,Q_d, as is often assumed. The two covariance matrices are thus:

$$Q_f = \alpha_f Q, \tag{26a}$$

$$Q_d = \alpha_d I, \tag{26b}$$

where Q is the matrix given by Equation 25 and I is the identity matrix. Each matrix is tuned with one fitting parameter, α_f and α_q, respectively, that is found by minimizing the SOC root mean square error (RMSE) on the US06 data. The RMSE is computed by:

$$RMSE = \sqrt{\frac{1}{N_t}\sum_{k=1}^{N_t}(SOC_k - SOC_k^{cc})^2} \tag{27}$$

where N_t is the number of time steps in the input profile. SOC^{cc} is the state-of-charge calculated from Coulomb counting,

$$SOC_k^{cc} = SOC_{k-1}^{cc} - \frac{\eta I(t) dt}{3600 Q_{nom}}, \tag{28}$$

where Q_{nom} is the nominal capacity of the cell and η is the Coulombic efficiency which is quantified as a function of C-rate by [10].

A primary function for the EKF in LIBs is to overcome initialization uncertainty, so the model was initialized with 3% SOC error to observe how each filter corrected the state. The voltage result for both filters is shown in Figure 5. The SOC RMSE is calculated to be 1.07% when using Q_f and 1.26% when using Q_d, showing very close performance.

V. Conclusions

This paper proposed an analytically-derived mapping method for quantifying process error (comprised of model uncertainty and process noise) in electrochemical LIB models. The eSPM model was first parameterized using experimental data from a 2 Ah 3.6 V Li-NMC cell, and a closed loop observer for the eSPM was formulated. Using the novel method for quantifying process error, it was shown that error in each state is roughly Gaussian, a sufficient condition that is often made but never verified. However, the assumption of uncorrelated process noise states, *i.e* a diagonal covariance matrix, was shown to be invalid, as all error states had a positive correlation. This was tested over the UDDS drive cycle and suggests that intercalation flux is the dominant source of model uncertainty for the data provided, as miscalculating it will cause all states within the particle to be off in the same direction. The covariance matrix

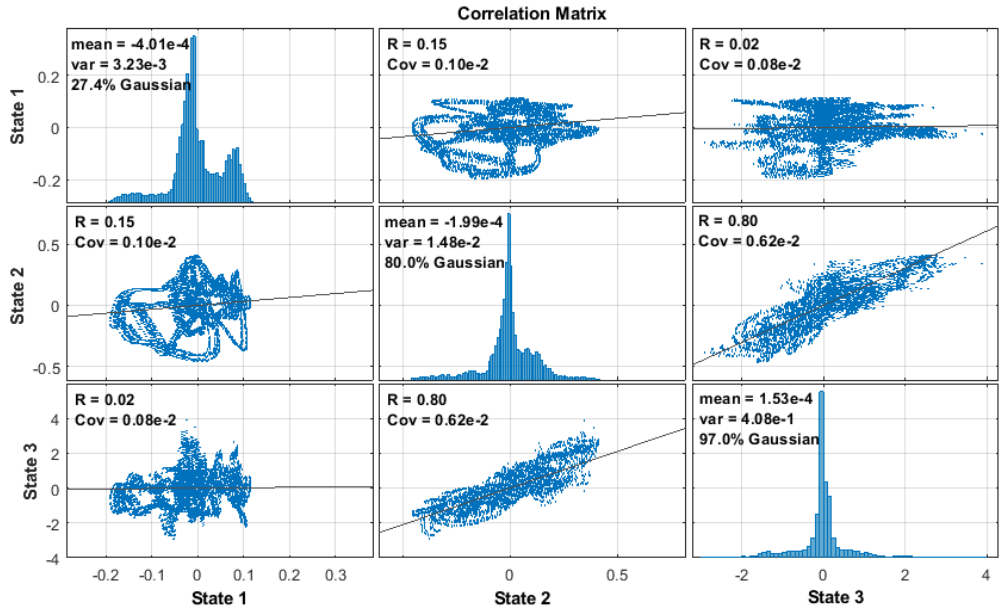

Fig. 4: Correlation plot of the process noise in each state. The mean, variance and z-test score are given for each state. The correlation coefficient, R, and covariance for each pair of states is given as well. Process noise for all states is positively correlated.

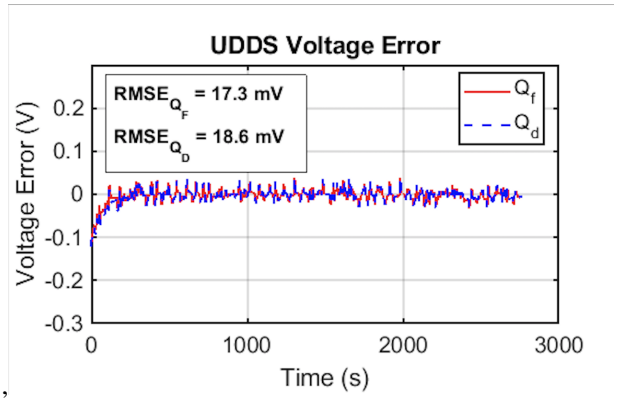

Fig. 5: Voltage profiles for both filters.

quantified using the proposed method overcame initialization uncertainty quicker and generally slightly outperformed the model which used a conventional diagonal covariance matrix. The method proposed in this work is not limited to LIB applications, as the idea of quantifying process error by ”mapping” a high-fidelity model so that it can be compared to a reduced one can be used in other engineering applications.

References

[1] R. Xiong, J. Cao, Q. Yu, H. He, and F. Sun, “Critical review on the battery state of charge estimation methods for electric vehicles,” *IEEE Access*, vol. 6, pp. 1832–1843, 2018.

[2] H. Rahimi-Eichi, U. Ojha, F. Baronti, and M.-Y. Chow, “Battery management system: An overview of its application in the smart grid and electric vehicles,” *IEEE Ind. Electron. Mag.*, vol. 7, no. 6, 2013.

[3] M. Dolye, T. Fuller, and J. Newman, “Modeling of galvanostatic charge and discharge of the lithium/polymer/insertion cell,” *Journal of The Electrochemical Society*, vol. 140, no. 6, p. 1526, 1993.

[4] T. Tanim, C. D. Rahn, and C. Wang, “State of charge estimation of a lithium ion cell based on a temperature dependent and electrolyte enhanced single particle model,” *Energy*, vol. 80, pp. 731–739, 2015.

[5] G. L. Plett, “Extended kalman filtering for battery management systems of lipb-based hev battery packs. part 3. state and parameter estimation,” *Journal of Power Sources*, vol. 134, pp. 277–292, 2004.

[6] D. D. Domenico, A. Stefanopoulou, and G. Fiengo, “Lithium-ion battery state of charge and critical surface charge estimation using an electrochemical model-based extended kalman filter,” *Journal of Dynamic Systems, Measurement, and Control*, vol. 132, 2010.

[7] B. Tjaden, S. J. Cooper, D. J. Brett, D. Kramer, and P. R. Shearing, “On the origin and application of the bruggeman correlation for analysing transport phenomena in electrochemical systems,” *Current Opinion in Chemical Engineering*, vol. 12, pp. 44 – 51, 2016.

[8] A. Allam and S. Onori, “An interconnected observer for concurrent estimation of bulk and surface concentration in the cathode and anode of a lithium-ion battery,” *IEEE Transactions on Industrial Electronics*, vol. 65, no. 9, 2018.

[9] S. Dey and B. Ayalew, “Real-time estimation of lithium-ion concentration in both electrodes of a lithium-ion battery cell utilizing electrochemical-thermal coupling,” *Journal of Dynamic Systems, Measurement, and Control*, vol. 139, pp. 031007–1–031007–10, 2017.

[10] H. He, X. Zhang, F. Sun, and J. Fan, “State-of-charge estimation of the lithium-ion battery using an adaptive extended kalman filter based on an improved thevenin model,” *IEEE Transactions on Vehicular Technology*, vol. 60, no. 4, 2011.